Multivoxel Proton MR Spectroscopy Reveals Subcortical Glial Response to SIV-Infection in Rhesus Macaques

William E. Wu[1], Ke Zhang[1], Assaf Tal[1], Eva-Maria Ratai[2], Ramon Gilberto Gonzalez[2], and Oded Gonen[1]

[1]*Radiology, New York University School of Medicine, New York, NY, United States,* [2]*Neuroradiology, Massachusetts General Hospital, Athinoula A. Martinos Center for Biomedical Imaging, Charlestown, MA, United States*

Target audience: HIV Clinicians. HIV/SIV Researchers. MR Spectroscopy Researchers. HIV-infected population.

Purpose: Although the success of highly-active antiretroviral therapy has dramatically reduced severe dementia in the million HIV-infected in the US, ≥50% of them will still suffer milder forms of HIV-associated neurocognitive disorders (HAND); these include memory impairment and planning difficulty which diminish quality of life (1). Histopathologic evidence from brains of HIV-seropositive patients with mild neurocognitive impairment corroborate HIV infection preferentially targets specific subcortical regions, e.g., putamen and hippocampus (2). It is not known in these patients whether injury to these areas is characterized by damage to the neurons, the glial cell populations, or both. These may be monitored via their proton MR spectroscopy (^{1}H-MRS) observed markers: *N*-acetylaspartate (NAA) for the neurons, *myo*-inositol (*m*I) for glia, and creatine (Cr) and choline (Cho) that are more abundant in the latter (3). Given HIV's predilection for subcortical areas and the myriad of toxic factors that can disrupt neuronal and glial function, our goal was to test in simian immunodeficiency virus (SIV)-infected rhesus macaques, an excellent animal model system (4), whether infection produces: *(a)* subcortical decreases in NAA; and/or *(b)* increases in glial markers, *m*I, Cho, and Cr. Towards these ends, we performed three-dimensional (3D) multivoxel ^{1}H-MRS at 0.125 cm^3 spatial resolution on five macaques before and 4-6 weeks after SIV-infection, and compared metabolite levels in six subcortical regions.

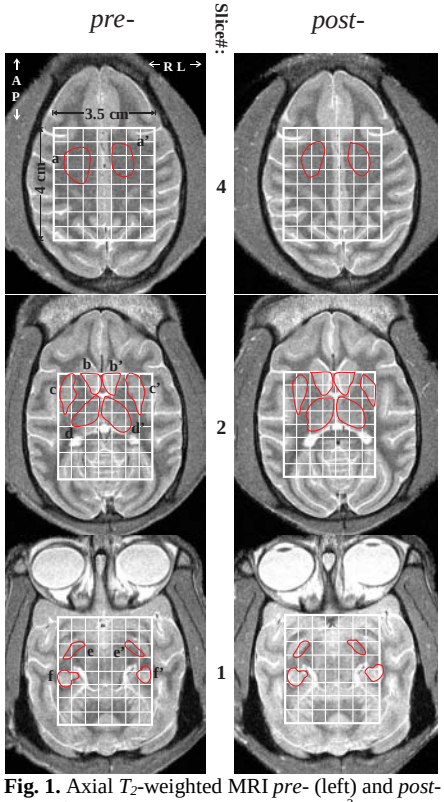

Fig. 1. Axial T_2-weighted MRI *pre-* (left) and *post-* SIV infection, showing the 3.5 × 4.0 cm^2 VOI (thick white frame), CSI grid (thin white lines) and six subcortical ROIs (red) where overlapping voxels' metabolite signals were averaged: centrum semiovale **(a, a')** in the white matter, caudate nucleus head **(b, b')**, putamen **(c, c')** and globus pallidus **(e, e')** of the basal ganglia, thalamus **(d, d')**, and hippocampus **(f, f')**.

Methods: All experiments were done in a 3-T MR imager (Magnetom TIM Trio, Siemens AG, Erlangen, Germany) with a circularly-polarized transmit-receive human knee coil. To guide placement of the ^{1}H-MRS volume-of-interest (VOI), sagittal and axial T_2-weighted turbo spin echo MRIs (TE/TR=16/7430 ms, 140×140 mm^2 field-of-view (FOV), 512×512 matrix, 2.0 mm sagittal and 1.2 mm axial slice thickness) were acquired. A 4.0 cm anterior-posterior (AP) × 3.5 cm left-right (LR) × 2.0 cm inferior-superior (IS) =28 cm^3 ^{1}H-MRS VOI was then centered on the corpus callosum. The VOI was excited using PRESS (TE/TR=33/1440 ms) with two 2nd-order Hadamard encoded slabs (four slices total) interleaved within every TR. These slices' planes were encoded with 16×16 2D-chemical shift imaging (CSI) over an 8×8 cm^2 (LR×AP) FOV to yield nominal (0.5 cm)^3 voxels, 224 of which fell in the VOI. These VOI spectra were each frequency-aligned and zero-order phased in reference to the NAA peak, then zero-filled to 256×256 in the time and chemical shift directions. Although zero-filling does not add new content to the raw data, it has been shown to increase spatial resolution by adding overlapping interpolated voxels, reducing partial volume effects (5). Relative levels of the i^{th} (NAA, Cr, Cho, *m*I) metabolite in the j^{th} animal were estimated from their peak areas, S_{ij}, using parametric spectral modeling and least-squares optimization software of Soher *et al.* (5). The S_{ij} were scaled into absolute concentrations by phantom replacement, as described previously (6). Cerebrospinal fluid (CSF) fraction within each region-of-interest (ROI) was calculated from segmented CSF masks using in-house software (MATLAB R2011b, Natlick, MA). To prevent underestimation due to CSF contributions metabolite values in each ROI were multiplied by 1/(1 - CSF fraction). Five (two females, three males; 5.0–8.6 kg weight) healthy rhesus macaques, all 3-4 years old, were scanned un-infected, then infected with SIV by intravenous injection, and rescanned 4-6 weeks later. Animals were under constant veterinary supervision. The protocol was approved by both Harvard Medical School and Massachusetts General Hospital IACUCs. Metabolite concentrations were estimated in six subcortical ROIs (shown in Fig. 1). Each ROI was outlined (bilaterally) on axial T_2-weighted MRI and overlaid on their corresponding spectral model functions using in-house software (IDL, Research Systems Inc., Boulder, CO). The software averaged all voxels that fell entirely or partially within the outlined areas. Paired sample *t* tests were used to assess the mean within-animal change in each metabolite from *pre-* to *post-*infection scans. Significance was tested at the $p<0.05$ level and SAS version 9.0 (SAS Institute, Cary, NC) was used for all calculations.

Results: *Pre-* to *post-*infection mean Cr increased 5%, 14%, and 9% in the putamen, globus pallidus, and thalamus, respectively: 8.2±0.9 to 8.6±1.2 mM, 6.9±0.7 to 7.9±0.9 mM, and 7.3±0.7 to 8.0±0.8 mM (all *p*-values ‹0.05); mean *m*I increased 18% in the thalamus: 7.1±0.9 to 8.3±0.7 mM ($p<0.05$). Slight increases at the "trend" level ($p\sim0.1$) were also observed in mean Cr of the centrum semiovale (+11%, 7.6±0.5 to 8.4±0.7 mM), and mean *m*I of the caudate nucleus and putamen (+16%, 7.0±1.3 to 8.1±0.6 mM, and +26%, 4.8±1.5 to 6.5±0.7 mM). No significant change was observed in mean Cho or NAA for any ROI. All within-animal ROI volume fraction changes were insignificant ($p>0.2$).

Discussion: SIV-infection produced glial activation notably in the thalamus, and more subtly in parts of the basal ganglia, as reflected by increases in glial markers, *m*I and Cr, in those regions, but overall neuronal health was not compromised, as shown by the lack of change in their marker, NAA, for all ROIs. These suggest that glial response (e.g., microglial activation, reactive astrocytosis), not neuronal damage, characterizes the injury to subcortical regions - at least during this stage of infection.

Conclusion: SIV-infection appears to cause subcortical brain injury indirectly, through glial activation, while neurons remain relatively intact. Treatment regimens aimed towards reducing gliosis may prove beneficial in preventing neuronal degeneration and associated neurocognitive impairment in patients with HAND. These results also suggest further study of the relationship between particular regions, e.g., thalamus, and brain injury in patients with HAND.

References: 1. Heaton RK, Marcotte TD, Mindt MR, et al. The impact of HIV-associated neuropsychological impairment on everyday functioning. *J Int Neuropsychol Soc* 2004;10(3):317-331. 2. Moore DJ, Masliah E, Rippeth JD, et al. Cortical and subcortical neurodegeneration is associated with HIV neurocognitive impairment. *AIDS* 2006;20(6):879-887. 3. Ross B, Bluml S. Magnetic resonance spectroscopy of the human brain. *Anat Rec* 2001;265(2):54-84. 4. Burudi EM, Fox HS. Simian immunodeficiency virus model of HIV-induced central nervous system dysfunction. *Adv Virus Res* 2001;56:435-468. 5. Soher BJ, Young K, Govindaraju V, Maudsley AA. Automated spectral analysis III. *Magn Reson Med* 1998;40(6):822-831. 6. Wu WE, Kirov, II, Zhang K, et al. Cross-sectional and longitudinal reproducibility of rhesus macaque brain metabolites. *Magn Reson Med* 2011;65(6):1522-1531.